



UBE3A controls axon initial segment in the cortical pyramidal neurons

Xinlang Liu^{a,1}, Zhuqian Jiang^{a,b,1}, Yoshinori Otani^a, Xiaowei Zhu^a, Yanyan Yu^a,
Abu Md Mamun Tarif^a, Raihana Nasrin Ferdousy^a, Tatsuya Kishino^c, Masashi Fujitani^{a,*}

^a Department of Anatomy and Neuroscience, Faculty of Medicine, Shimane University, Izumo, 693-8501, Japan

^b Ningxia Key Laboratory of Craniocerebral Diseases, Ningxia Medical University, 1160 Shengli Street, Yinchuan, 750004, Ningxia, China

^c Division of Functional Genomics, Graduate School of Biomedical Sciences, Nagasaki University, Nagasaki, Japan

ARTICLE INFO

Keywords:

Axon initial segment
Ubiquitin-protein ligase E3A
Angelman syndrome
Prelimbic cortex
Pyramidal neurons

ABSTRACT

The axon initial segment (AIS) is a critical regulator of neuronal excitability and the initiation site of action potentials. Alterations in the structural features of AIS, such as length and position, have been shown to influence neuronal function, a phenomenon known as activity-dependent AIS plasticity. In addition to their physiological functions, abnormalities in the AIS have been implicated in various neurological disorders. UBE3A is an E3 ubiquitin ligase crucial for protein degradation in neurons. In mature neurons, only the maternal allele of the *UBE3A* gene is active, and the paternal allele is silenced. However, the role of UBE3A in controlling AIS in the cortical pyramidal neurons has not yet been fully elucidated. In this study, we compared wild-type mice with three different *Ube3a*-deficient mice and observed specific elongation of the AIS in the prefrontal cortex of the medial prefrontal cortex but not in the somatosensory cortex or motor cortex, as previously reported. Interestingly, we also showed that UBE3A controls AIS length in a cell-autonomous manner using cultured cortical neurons derived from *Ube3a*-floxed (*Ube3a^{fllox/fllox}*) mice. This study indicates that UBE3A controls AIS length through a cell-autonomous mechanism *in vitro*. However, non-cell-autonomous mechanisms, including feedback from inhibitory neurons or connections with the hippocampus, may also influence adult AIS length *in vivo*, thereby helping to maintain the excitability homeostasis of cortical pyramidal neurons in a region-specific manner.

1. Introduction

The axon initial segment (AIS) is a critical regulator of neuronal excitability, which serves as an initiation site for action potentials (APs) [1–3]. Alterations in the structural features of AIS, including in the length and position, have been shown to influence neuronal function [4–6]. This physiological phenomenon, termed activity-dependent AIS plasticity [7,8], has also been observed in sensory neurons receiving tactile [9], auditory [5], olfactory [10] and visionary inputs [11]. Beyond its physiological roles, a growing body of research has linked AIS abnormalities to a wide variety of neurodegenerative, neuropsychiatric disorders, amyotrophic lateral sclerosis (ALS) [12], Alzheimer's disease [13], autism spectrum disorder (ASD) [14], attention-deficit hyperactivity disorder (ADHD) [15], Fragile-X syndrome [16] and Angelman

syndrome (AS) in model mice [17].

The *UBE3A* gene encodes the E3 ubiquitin ligase E3A (UBE3A), which is crucial for protein degradation in neurons [18,19]. Although paternal *Ube3a* is expressed in immature neurons during the first post-natal week [20], in mature neurons, *Ube3a* expression is uniquely regulated by genomic imprinting, in which only the maternal allele is active and the paternal allele is silenced [21,22]. This selective expression is crucial for normal neuronal function and development [20]. UBE3A plays an important role in synaptic development and plasticity by regulating synaptic proteins [18,19]. However, the function of UBE3A remains elusive.

Disruptions in maternally expressed *UBE3A* cause a disorder termed AS, a neurodevelopmental disorder characterized by severe cognitive impairment, ataxia, speech difficulties, and frequent seizures [21,22]. In

Abbreviations: AIS, Axon initial segment; UBE3A, Ubiquitin-protein ligase E3A; AS, Angelman syndrome; WT, Wild-type; mKO, heterozygous *Ube3a* maternal deficient mouse; pKO, heterozygous *Ube3a* paternal deficient mouse; fKO, homozygous *Ube3a* biallelic (full) deficient mouse; mPFC, medial prefrontal cortex; PrL, Prelimbic cortex; PyNs, Pyramidal neurons; SC, Somatosensory cortex; MC, Motor cortex; AAV, Adeno-associated virus.

* Corresponding author. Department of Anatomy and Neuroscience, Faculty of Medicine, Shimane University 89-1 Enya-cho, Izumo-shi, Shimane 693-8501, Japan.

E-mail address: fujitani@med.shimane-u.ac.jp (M. Fujitani).

¹ These authors contributed equally to this work.

<https://doi.org/10.1016/j.bbrc.2025.151429>

Received 31 October 2024; Received in revised form 30 January 2025; Accepted 30 January 2025

Available online 1 February 2025

0006-291X/© 2025 Elsevier Inc. All rights are reserved, including those for text and data mining, AI training, and similar technologies.

previous animal studies, Kaphzan et al. reported AIS elongation in the CA1 pyramidal neurons (PyNs) of the hippocampus in an AS model, heterozygous *Ube3a* maternal-deficient (mKO) mice, with disruption of exons 1 and 2 [17]. They also showed that the length of the AIS in layer V pyramidal neurons of the somatosensory cortex (SC) remained unchanged [23]. However, alterations in AIS in other cortical areas remain unclear.

We analyzed the AIS length in four different brain areas of four genotypes of mice: wild-type (WT), mKO, heterozygous *Ube3a* paternal-deficient (pKO), and homozygous *Ube3a* biallelic (full)-deficient mice (fKO), with disruptions in exons 15 and 16. We further examined the cell-autonomous functions of UBE3A in cultured cortical neurons extracted from *Ube3a*-floxed (*Ube3a*^{fllox/fllox}) mice.

2. Materials and methods

2.1. Mice

Mutant mice were generated by deleting part of exons 15 and 16 from the C57BL6/J background [24] and were reared at Nagasaki University. fKO mice were generated by crossing heterozygous male *Ube3a*-deficient mice with heterozygous female *Ube3a*-deficient mice. This breeding strategy generated four experimental groups: WT, mKO, pKO, and fKO mice. *Ube3a*^{tm1a(KOMP)Wtsi} (MGI ID: 4419739; MMRRC ID: 37375) was purchased from the Mutant Mouse Resource and Research Center (MMRRC, USA) of Jackson Laboratories. B6-Tg(CAG-FLPe)36 (RBRC018134) mice were obtained from RIKEN BioResource Research Center (BRC, Japan). Mouse tail genomic DNA was genotyped using GoTaq Green Master Mix (Promega, Madison, WI, USA) with the following primers: *Ube3a*-15F, GGAGTTCTGGGAAATTGTTCA; En2-R, CACGCCATACAGTCTCTTC; *Ube* (37375) F, AAAATTGGGTATGC-GAGCTG; *Ube* (37375) R, GGGGTCTAAGGGCCTATGAA; and 5CAG, CCTACAGCTCCTGGCAACGTGC. R: CTGCTTCTCCGATGATTCG; oIMR0042: CTAGGCCACAGAATTGAAAGATCT; oIMR0043: GTAGGTGAAATTCTAGCATCATCC. PCR conditions were as follows: pre-denaturation at 95 °C for 2 min and 30 amplification cycles (95 °C for 30 s; 58 °C for 30 s; extension at 72 °C for 30 s) and final additional extension at 72 °C for 5 min. All mice were maintained in a specialized transgenic mouse room at the Department of Experimental Animals, Interdisciplinary Center for Science Research, Head Office for Research and Academic Information, Shimane University, following the university guidelines for the care and use of animals. All animal experiments were approved by the Department of Experimental Animals, Interdisciplinary Center for Science Research, Head Office for Research and Academic Information, Shimane University (approval numbers: IZ4-4, IZ4-12, and IZ4-35).

2.2. Immunofluorescence staining

Eight-week-old male *Ube3a* deficient mice were intraperitoneally injected with a combination of medetomidine (0.3 mg/kg, Meiji Animal Health Pharma Co., Tokyo, Japan), midazolam (4.0 mg/kg, Maruishi Pharmaceutical Co., Osaka, Japan), and butorphanol (5 mg/kg; Meiji Animal Health Pharma Co., Tokyo, Japan). Following cardiac perfusion fixation with 4 % paraformaldehyde (PFA) in 0.01 M phosphate buffer saline (PBS; pH 7.4), the brains were extracted and post-fixed on ice for 2 h (4 % PFA). After fixation, the brains were rinsed with saline and immersed in 30 % sucrose in PBS at 4 °C overnight. Following sucrose replacement, the brains were sectioned into 50 µm coronal sections using a freezing sliding microtome (HM430, Thermo Fisher Scientific, Waltham, MA, USA). Antigen retrieval was performed in 0.01 M citrate buffer (pH 6.0) using a microwave oven; the buffer was first boiled, and then incubate for 30 min on 25 °C. Brain slices were blocked with 0.4 % Triton X-100 and 3 % normal donkey serum (NDS) in 0.01 M PBS for 1 h. The sections were incubated for two nights at 4 °C in primary antibody diluted to an appropriate concentration in blocking buffer. The samples

were then thoroughly washed in PBST, followed by incubation with fluorescently labeled secondary antibodies overnight at 4 °C. Residual secondary antibodies were washed off with PBST. The samples were placed on gelatin-coated glass slides and covered with glass coverslips using a Fluorescence Mounting Medium (S3023, Dako). *In vitro*, primary cortical neurons were fixed with 4 % PFA for 15 min at 4 °C and permeabilized with 0.1 % Triton X-100 in PBS for 5 min. After blocking with 3 % NDS for 30 min at 25 °C, cells were incubated with primary antibody overnight at 4 °C, and with fluorescently labeled secondary antibodies for 2 h at 25 °C in the dark. Cover glasses were mounted on glass slides using Vibrance Antifade Mounting Medium (Vector Laboratories, Burlingame, CA, USA, #H-1700). The following are the antibodies used and their dilution ratios: Anti-Ankyrin-G (1:1000, Mouse, NeuroMab Davis, #75-146); Anti-COUP TF1-interacting protein 2 (CTIP2) antibody (1:1000, Rat, Abcam, #ab18465); Anti-MAP2 antibody (1:1000, Rabbit, Cell Signaling Technology, #7870); NeuroTrace® Green 500/525 Fluorescent Nissl Stain (1:250, Molecular probes/Thermo Fisher Scientific); Donkey anti-mouse IgG (H + L) Alexa Fluor 647 plus (1:1000, Molecular probes/Thermo Fisher Scientific, #A32787); Donkey anti-rabbit IgG (H + L) Alexa Fluor 405 plus (1:500, Molecular probes/Thermo Fisher Scientific, #A48258); Donkey anti-rat IgG (H + L) Cy3 conjugated (1:1000, Jackson ImmunoResearch Laboratories #712-165-153).

2.3. AIS imaging and analysis

All brain slice images were obtained using FV-1000D and FV-3000D confocal microscopes (Olympus, Tokyo, Japan) with 60X (Numerical Aperture (NA) = 1.30) oil immersion and 40X (NA = 1.25) objectives, and appropriate laser excitation and filters. Four fields of view were captured for each area. The image size was 1024 × 1024 pixels, with 4.9010 µm/pixel XY resolution, and Z steps of 1 µm. Cultured neuronal images were acquired using a 40X oil-immersion objective, appropriate laser excitation, and filters. The image size was 1024 × 1024 pixels with an XY resolution of 3.2834 µm/pixel. All 3D images were measured automatically using the Simple Neurite Tracer plugin in ImageJ after manually specifying the start and end points of the AIS in Z-stack images [25].

2.4. Adeno-associated virus (AAV) vector preparation

The target plasmid (10 ng) was added to 50 µL of competent cells, and placed on ice for 30 min, followed by heat shock in a 42 °C water bath for 45 s, and then placed on ice for 1 min. SOC medium (450 µL) was added to the cells and incubated in a 37 °C water bath for 1 h. The transformation mixture (100 µL) was subsequently inoculated onto LB agar plates containing ampicillin and incubated overnight at 37 °C. A single colony from the agar plate was then picked and placed in 5 mL LB broth containing the same antibiotics and cultured at 37 °C with shaking overnight until the logarithmic growth phase. Subsequently, the suspension was inoculated into 100 mL LB liquid culture medium at a ratio of 1:1000 and culture at 37 °C with shaking for 24 h. Plasmid DNA purification using NucleoBond® Xtra Midi/Maxi kits (TaKaRa Bio, #740410.10) referring to the instruction manual Maxi. The purity and concentration of the isolated plasmids were determined using spectrophotometry. The AAV vector was prepared as follows: The fully confluent HEK293T cells were subculture in a 10 cm dish in two PLL-coated 10 cm dishes; The volume of culture medium in each 10 cm dish; Then proceed with transfection once the cells reach approximately 70–80 % confluency; A DNA mixture was prepared using expression vector (pAAV2-CAG-EGFP(enhanced green fluorescent protein) 6 µg or pENN.AAV.hSyn.HI. eGFP (enhanced GFP)-Cre.WPRE.SV40 6 µg) with pHelper Vector 10 µg and pUCmini-iCAP-AAV9-x1.1 12 µg in 1 mL Dulbecco's Modified Eagle's medium (DMEM)-high glucose (without fetal bovine serum [FBS]), respectively. To enhance cellular uptake, 1 mg/mL polyethyleneimine (PEI) was added at a 1:2 ratio of DNA to PEI.

The complex was incubated for 30 min at 25 °C, after which 1 mL of the PEI-DNA complex was added to 8 mL of DMEM with FBS and added dropwise to cells. After 24 h, the medium was aspirated and 10 mL of DMEM without FBS was added and incubated for 5 days. After eight days, the cell supernatant containing the AAV vector was collected. Block Vivaspin 20 (1,000,000 MWCO, VS2041, Sartorius) with 5 mL 1 % BSA/PBS for 15 min and centrifuge at 800×g for 2 min at 25 °C. The flow-through was aspirated and 1 % BSA/PBS was left on top. PBS (5 mL) was added, and the mixture was centrifuged at 800×g for 2 min. The flow-through was aspirated, and PBS was left on top. The entire volume of the medium was placed in a 50 mL tube and centrifuged at 800×g for 5 min at 25 °C. The supernatant was collected and filtered using a 0.45 µm filter. The medium containing AAV were added to the Vivaspin 20 and centrifuged at 2600×g for 45–70 min at 4 °C until the volume is approximately 1 mL. Add PBS (15 mL) was added and centrifuged and this step was repeated until concentrate until the volume of 200–500 µL. Subsequently, the sample was transferred to a 1.5 mL loop screw cap tube. Genomic titer measurements were finally performed using real-time PCR.

2.5. Primary cortical neuron culture

On embryonic day 14.5 (E14.5), pregnant *Ube3a^{flox/flox}* mice were sacrificed using carbon dioxide in a CO₂ chamber. The abdominal skin was disinfected with 70 % ethanol and cut with surgical scissors. Embryos were quickly retrieved from the uterus, and transferred to pre-cooled Hank's balanced salt solution (Fujifilm Wako Pure Chemical Corporation, #085–09355) containing an antibiotic-antimycotic (Invitrogen, #15240062) (HBSS-AA). The heads were decapitated and immediately transferred to a 6 cm Petri dish containing ice-cold HBSS-AA. The cortex was quickly peeled away, and the meninges were completely removed under a dissecting microscope, and cut into smaller pieces using a scalpel blade. Once all of the cortices were dissected, they were transferred to pre-warmed DMEM-high glucose (Sigma-Aldrich, #D5796) with papain (0.5 mg/mL Fujifilm Wako Pure Chemical Corporation, #164–00172), DNaseI (0.1 mg/mL, Sigma, #DN25), and digested in a cell culture incubator for 30 min at 37 °C. FBS (10 %, HyClone™, SH30910.03, Cytiva, England) was added to stop digestion. A sterile glass Pasteur pipette was used to triturate the cortical neurons to completely dissociate them, after which the resulting mixture was filtered into a 50 mL centrifuge tube using a 70 µm filter. After centrifugation at 300×g for 5 min, the supernatant was aspirated, and the cell pellet was resuspended in culture medium consisting of B-27 Plus Neuronal Culture System (Invitrogen, #A3653401), penicillin-streptomycin (1x, PS, FUJIFILM Wako, #168–23191) + L-Alanyl-L-Glutamine Solution (2 mM, FUJIFILM Wako, #016–21841). Trypan Blue was used for cell counting and then seeding at a density of 40,000 cells/cover slip onto 13 mm diameter coverslips in 4 well plates pre-coated with Poly-L-ornithine (0.1 mg/mL, Sigma, #P3655-50 MG) + Fibronectin (10 µg/mL, Corning, #356008). Cell culture plates were incubated at 37 °C with 5 % CO₂. The following day, half of the medium was replaced with AAV at an MOI of 10⁴, gently mixed, and placed in an incubator. For all coverslips, the 250 µL of medium was aspirated 48 h after infection. Complete aspiration of the medium was avoided to prevent oxidative damage to the neurons, and 300 µL of new preheated medium was rapidly added. Fluorescence microscopy BZ-X700 (Keyence, Tokyo, Japan) with 10X (NA = 0.45) objective (image size: 1920×1440 pixels), was applied to determine the infection efficiency of AAV in target cells. Immunofluorescence staining was performed at seven DIV (days *in vitro*).

2.6. Statistical analysis

All statistical analyses were performed with the GraphPad Prism software version 9.5.1 (GraphPad Software, Boston, MA, USA), and presented as mean ± standard error (SEM). Prism tests the assumption

with Brown-Forsythe test for one-way analysis of variance (ANOVA), and F test to compare variances for the unpaired *t*-test. Significance was assessed using unpaired *t*-tests for two-group comparisons, one-way ANOVA, and Tukey's multiple tests for comparisons among three or more groups. Differences were considered statistically significant at *p* < 0.05 for each statistical method. To calculate the effect size of ANOVA (eta squared, η^2), the following calculation was performed:

$$\eta^2 = \frac{SS_A}{SS_T}$$

SS_A is between columns of the Sum of Squares (SS) and SS_T is the total SS.

3. Results

3.1. Altered AIS length of layer V pyramidal neurons (PyNs) in prefrontal cortex (PrL) of mKO and fKO mice

To assess the AIS length, we first aimed to clearly visualize the three-dimensional morphology of PyNs in the cortex using confocal 3D imaging (Fig. 1A). We evaluated this method using NeuroTrace® as a marker for the whole cell bodies of PyNs, CTIP2 for layer V PyNs, and Ankyrin-G for AIS. As shown in Fig. 1A, all the markers produced clear signals. Therefore, we used these markers to quantify AIS length. We quantified the AIS length in the layer V PyNs of WT, mKO, pKO, and fKO mice. mKO mice are commonly used as AS models. Compared to WT mice, we observed an increase in the AIS length of layer V PyNs of PrL only in mKO and fKO mice, but no abnormalities were observed in the AIS of pKO mice (WT: 26.46 ± 0.1864 µm; mKO: 30.40 ± 0.2564 µm; pKO: 26.32 ± 0.2289 µm; fKO: 30.76 ± 0.1414 µm, *F* = 135.9, *p* < 0.0001, η^2 = 0.9713) (Fig. 1B). The cumulative frequency distribution plot of individual AIS lengths showed a rightward shift with no change in shape in layer V of the PrL in mKO and fKO mice. However, pKO mice did not show any shift compared to WT mice (Fig. 1C). These results indicate the importance of the maternal allele of the *Ube3a* gene for the regulation of AIS in PrL.

3.2. The AIS of layer V PyNs in the SC and motor cortex is not altered in *Ube3a*-deficient mice

We subsequently investigated whether AIS abnormalities were present in layer V PyNs in the primary motor cortex (M1), secondary motor cortex (M2), and SC of WT mice (Fig. 2A). We found that PyNs in layer V of M2 have significantly longer AIS than M1 or SC (PrL: 26.46 ± 0.1864 µm; M1: 24.84 ± 0.4883 µm; M2: 27.59 ± 0.9790 µm, SC: 24.56 ± 0.6582 µm, *F* = 4.867, *p* = 0.0193, η^2 = 0.5489). We further compared the results between WT and *Ube3a*-deficient mice. Representative confocal images of the coronal sections are presented in Supplementary Fig. 1. We found no significant differences in AIS length between WT and any other mutant mice in M1, M2 and SC (M1: WT: 24.84 ± 0.4883 µm, mKO: 23.96 ± 0.9313 µm, pKO: 24.71 ± 0.4454 µm, fKO: 25.04 ± 0.7354 µm, *F* = 0.4843, *p* = 0.6994, η^2 = 0.1080; M2: WT: 27.59 ± 0.9790 µm, mKO: 27.75 ± 0.9441 µm, pKO: 26.87 ± 0.6218 µm, fKO: 28.26 ± 1.198 µm, *F* = 0.3606, *p* = 0.7826, η^2 = 0.0827; SC: WT: 24.56 ± 0.6582 µm, mKO: 25.42 ± 0.7507 µm, pKO: 23.70 ± 0.3029 µm, fKO: 25.90 ± 0.7582 µm, *F* = 2.254, *p* = 0.1344, η^2 = 0.3605) (Fig. 2B, C and D). Cumulative frequency distribution plots of individual AIS lengths showed no changes in shape or shifts in layer V PyNs of the MC and SC in mKO, pKO, and fKO mice compared to WT mice (Fig. 2B, C, and D).

3.3. AAV-mediated *Ube3a* deletion elongates AIS length in primary cortical neurons

To investigate whether abnormal AIS length in the PrL occurs cell-autonomously or via neurocircuit-dependent non-cell-autonomous

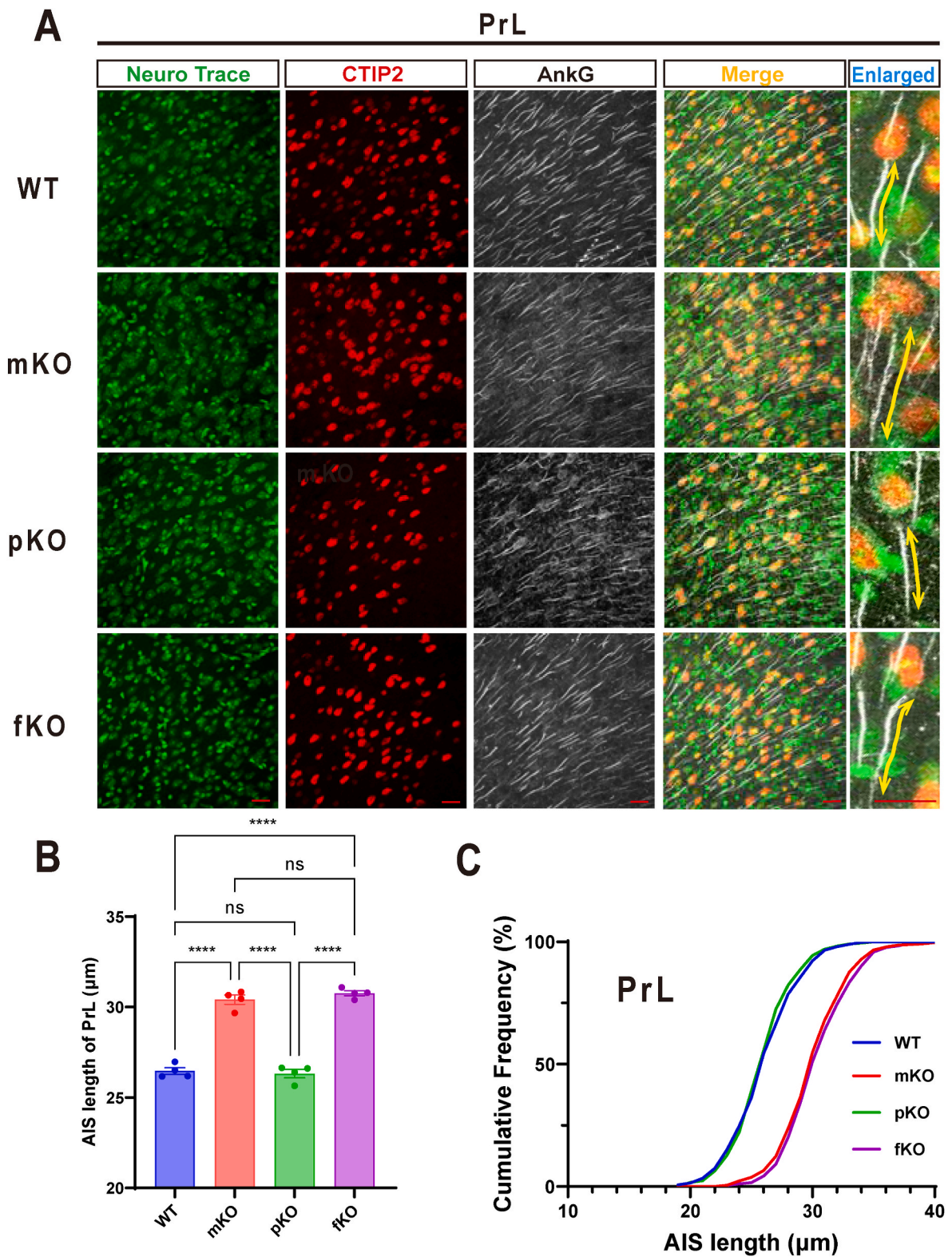
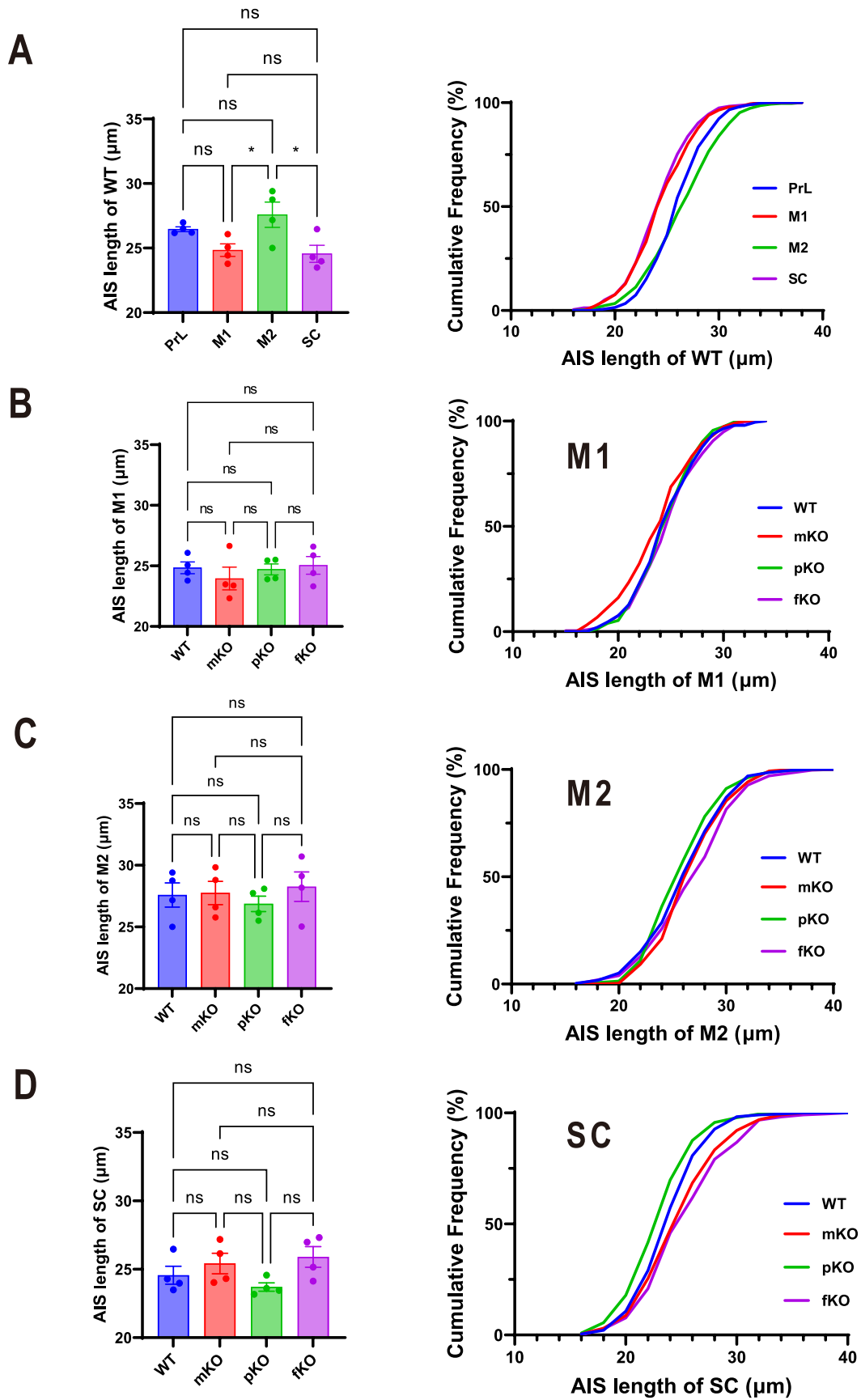


Fig. 1. Heterozygous *Ube3a* maternal-deficient (mKO) and homozygous *Ube3a* biallelic-deficient mice (fKO) show increased axon initial segment (AIS) length of layer V pyramidal neurons (PyNs) in the prelimbic cortex (PrL).

A) Representative confocal stacks images of coronal sections and high-magnification of a layer V PyN in PrL labeled for fluorescent Nissl (NeuroTrace®, green), COUP TF1-interacting protein 2 (CTIP2, red), and Ankyrin-G (AnkG, white). Scale bar = 20 µm. **B)** Quantification histogram of AIS length of wild-type (WT, n = 416 cells, 4 mice), heterozygous *Ube3a* maternal-deficient (mKO, n = 397 cells, 4 mice), heterozygous *Ube3a* paternal-deficient (pKO, n = 468 cells, 4 mice), and homozygous *Ube3a* biallelic-deficient mice (fKO, n = 439 cells, 4 mice). Data were shown as mean ± standard error (SEM) and group comparisons were performed using one-way analysis of variance (ANOVA), followed by Tukey's multiple comparison tests. n.s., not significant; ****p < 0.0001. **C)** Cumulative frequency of AIS length across all PyNs in PrL examined for each genotype. (For interpretation of the references to colour in this figure legend, the reader is referred to the Web version of this article.)



(caption on next page)

Fig. 2. *Ube3a* deficient mice show no aberrant axon initial segment (AIS) length of layer V pyramidal neurons (PyNs) in the primary motor cortex (M1), the secondary motor cortex (M2), and somatosensory cortex (SC).

A) Quantification histogram and cumulative frequency of AIS length of layer V PyNs in PrL, M1, M2 and SC of wild type (WT) mice (PrL: $n = 416$ cells; M1: $n = 196$ cells; M2: $n = 293$ cells; SC: $n = 234$ cells; each group = 4 mice). **B)** Quantification histogram and cumulative frequency of AIS length of layer V PyNs in M1 of wild-type (WT), *Ube3a* maternal-deficient (mKO), *Ube3a* paternal-deficient (pKO), and *Ube3a* biallelic-deficient mice (fKO) mice (M1: WT, $n = 196$ cells; mKO: $n = 192$ cells; pKO: $n = 227$ cells; fKO: $n = 235$ cells; each group = 4 mice). **C)** Quantification histogram and cumulative frequency of AIS length of layer V PyNs in M2 examined for each genotype (M2: WT, $n = 293$ cells; mKO: $n = 294$ cells; pKO: $n = 293$ cells; fKO: $n = 302$ cells, each group = 4 mice). **D)** Quantification histogram and cumulative frequency of AIS length of layer V PyNs in SC examined for each genotype (SC: WT, $n = 234$ cells; mKO: $n = 228$ cells; pKO: $n = 235$ cells; fKO: $n = 220$ cells, each group = 4 mice). Data are shown as mean \pm standard error (SEM) and group comparisons are performed using one-way analysis of variance (ANOVA), followed by Tukey's multiple comparison tests. n.s., not significant; **** $p < 0.0001$.

mechanisms, we generated *Ube3a*^{fllox/fllox} mice by mating *Ube3a*^{tm1a} (*KOMP*)^{Wtsi} and B6-Tg (CAG-FLPe) mice (Fig. 3A). After establishing a culture of cortical neurons from *Ube3a*^{fllox/fllox} E14.5 mice, we infected neurons with AAV-EGFP as a control or AAV-Cre-eGFP to ablate the *Ube3a* gene. As presented in Fig. 3A and B, EGFP was expressed throughout the cell body, whereas Cre-eGFP was localized to the neuronal nuclei. Cultured neurons were immunostained for MAP2 as a neuronal marker and Ankyrin-G to visualize AIS. Subsequently, AIS length was quantified in neurons expressing EGFP or Cre-eGFP (Fig. 3A and B). Immunohistochemical analysis at 6 days after post-AAV infection showed approximately 3.5 μm significant increase in AIS length in *Ube3a*^{fllox/fllox} neurons that received AAV-Cre-eGFP infection compared to that *Ube3a*^{fllox/fllox} cortical neurons received AAV-EGFP control vector (AAV-EGFP: $29.56 \pm 0.4975 \mu\text{m}$; AAV-Cre-eGFP: $33.03 \pm 0.6944 \mu\text{m}$). These results indicated that *Ube3a* deficiency altered the length of the AIS *in vitro* (Fig. 3C).

4. Discussion

In the present study, we showed that the AIS length of layer V PyNs in the PrL of mKO and fKO mice was specifically elongated, indicating hyperexcitability of these neurons. In contrast, the AIS of layer V PyNs in the SC and MC remained unchanged in all *Ube3a*-deficient mice, which is consistent with prior reports [17,23]. In WT mice, the AIS length differed significantly between the PrL, MC, and SC. Furthermore, AAV-mediated *Ube3a* deletion resulted in AIS elongation in primary cortical neurons, indicating increased excitability of cultured cortical neurons.

Because paternal UBE3A is expressed in immature neurons during the first postnatal week, whereas mature neurons do not express detectable levels of paternal UBE3A [20], we examined whether postnatal paternal UBE3A affects the development of AIS in developing neurons. To investigate this, we compared the AIS lengths in the brains of four mouse genotypes (WT, mKO, pKO, and fKO). As shown in Figs. 1 and 2, we detected AIS elongation in the PrL layer V PyNs of mKO and fKO mice, but not in pKO mice. These results led us to conclude that the paternal UBE3A protein does not influence the development of PyNs in the cortex, and that the AIS of PyNs in mKO mice is essentially the same as that in fKO mice.

We further demonstrated that UBE3A regulates AIS in cortical neurons in a cell-autonomous manner (Fig. 3), as previously observed in hippocampal neurons [17]. However, the mechanisms by which UBE3A affected the development of AIS are not entirely clear. During the early stages of AIS development, preceding the assembly of the AIS molecular structure, a periodic actin-spectrin scaffold forms immediately after axonal specification [26]. In cortical neurons, Ankyrin-B and β II-spectrin initially assemble in the distal axon, followed by clustering of Ankyrin-G in the proximal region, where β IV-spectrin eventually replaces or supplements β II-spectrin [27]. Full-length Ankyrin-G (480 kDa) is essential for recruiting other AIS components, such as ion channels, cell adhesion molecules, and β IV-spectrin [28,29]. These findings highlight a stepwise and hierarchical process of AIS formation, and suggest that these proteins could be targets of UBE3A. In support of this idea, previous studies have shown that UBE3A deficiency can induce the upregulation of AIS related proteins, such as Ankyrin-G and Na_v1.6 [17] via an α 1 subunit of

Na/K-ATPase dependent mechanism [30], but only in the hippocampus, not in the cortex [17].

To further explore the molecular mechanisms of action of this protein, we analyzed the overlap between AIS-localized proteins in neurons, recently determined by the immunoproximity biotinylation method [31], and previously reported substrates of UBE3A [19], as well as all candidates identified by orthogonal ubiquitin transfer (OUT) method in HEK (human embryonic kidney) 293 cells [32], and in an assay involving the isolation of interacting proteins using stringent washes in *Drosophila* neural tissues [33]. However, we found no overlap between these datasets (data not shown).

Another candidate is the calcium- and voltage-dependent big potassium (BK) channel, a known substrate of UBE3A [34]. UBE3A deficiency led to increased BK channel activity and elevated intrinsic excitability in individual neurons, potentially contributing to AIS elongation. Furthermore, BK channels interact with Na_v1.2 and modulate action potential generation in AIS [35]. As such, this channel may be a relevant substrate for UBE3A.

Despite these analyses, a critical question remained: Why is the AIS of layer V PyNs in the PrL specifically elongated in adult mKO and fKO mice? If neuronal changes are governed by a purely cell-autonomous mechanism throughout development, it is unlikely that only the AIS of layer V PyNs in the PrL would be affected. Loss of UBE3A may result in elongation of the AIS in all excitatory neurons during early development. However, adult AIS length can be modulated during developmental processes, such as in the visual cortex (VC) [11] and SC [9]. As such, we propose the hypothesis (illustrated in Fig. 4) that both local inhibitory-excitatory circuits and long-range neuronal connections are affected by UBE3A deficiency.

Previous data have suggested that the loss of UBE3A leads to intrinsic hyperexcitability in CA1 and CA3 neurons of the hippocampus, accompanied by a longer AIS [17]. In addition, a previous report showed that the loss of UBE3A leads to decreased excitability of layer V fast-spiking interneurons in the medial prefrontal cortex (mPFC) [36], whereas another study observed increased intrinsic excitability of layer II/III pyramidal neurons and decreased inhibitory synapses without reduced interneuron excitability [37].

A unique type of GABAergic axoaxonic synapse forms in AIS, controlling the neuronal output [38]. These synapses are formed by a specific inhibitory neuronal group comprising fast-spiking interneurons and chandelier cells (ChCs) [39]. ChCs are predominantly found in layers II/III of the dorsolateral prefrontal cortex, SC, MC, VC, and the CA1 and CA3 regions of the hippocampus [40]. Hence, the diversity of interneurons may underlie different regional phenotypes [41]. In contrast, a recent connectome study found that the mPFC receives significant input from the hippocampus [42]. These observations suggest that hyperexcitability in the hippocampus may drive greater activation of mPFC layer V PyNs than in other areas, potentially elongating AIS. Such changes may further help to maintain excitability homeostasis in the cortical pyramidal neurons in a region-specific manner.

The PrL in rodents is a crucial area of the mPFC that controls higher brain functions, including cognition, emotion, reward, and motivation [43,44]. The mPFC is also involved in ASD, anxiety, depression, and ADHD [43,44]. Several animal models of AS have presented with phenotypes that mimic patient symptoms such as cognitive impairment,

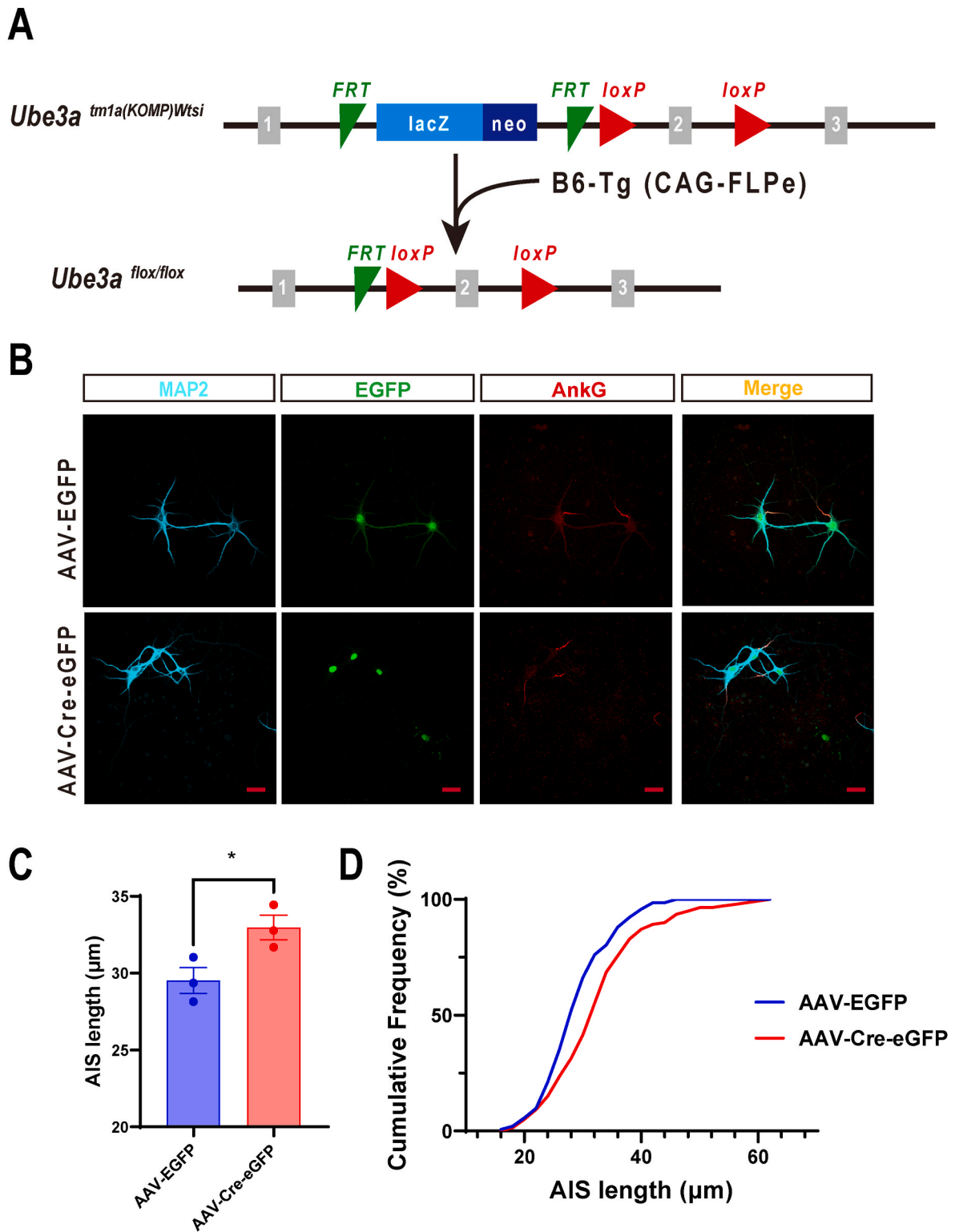


Fig. 3. Elongated axon initial segment (AIS) length is induced by Adeno-associated virus (AAV)-mediated *Ube3a* deletion in primary cortical neurons. **A)** Strategy for generating *Ube3a*-floxed (*Ube3a*^{flox/flox}) mice. **B)** Representative confocal images of AIS of primary cortical neurons from E14.5 *Ube3a*^{flox/flox} mice labeled for Microtubule-associated protein 2 (MAP2, blue), enhanced green fluorescent protein (EGFP, green), and Ankyrin-G (AnkG, red). Scale bar = 30 µm. **C)** Quantification histogram of AIS length of AAV-EGFP and AAV-Cre-eGFP infected primary cortical neurons derived from E14.5 *Ube3a*^{flox/flox} mice (AAV-EGFP: n = 143 cells; AAV-Cre-eGFP: n = 140 cells; each group = 3 mice). Data are shown as mean ± standard error (SEM) and group comparisons are performed using the independent samples *t*-test. **p* < 0.05. **D)** Cumulative frequency of AIS length of all primary cortical neurons examined for AAV-EGFP and AAV-Cre-eGFP. (For interpretation of the references to colour in this figure legend, the reader is referred to the Web version of this article.)

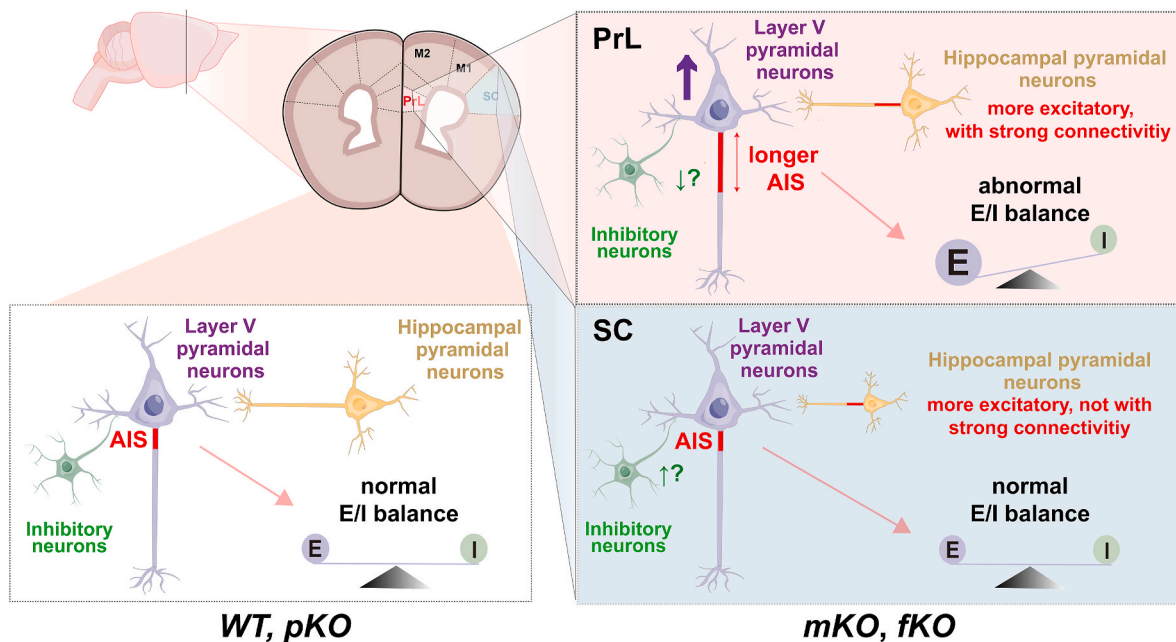


Fig. 4. A schematic illustrating the proposed role of UBE3A in different cortical regions. The loss of UBE3A may lead to elongation of the axon initial segment (AIS) in all excitatory neurons only during early development via a cell autonomous mechanism. However, as development progresses in the adult brain, local inhibitory–excitatory circuits and long-range neuronal connections can influence the excitability of layer V pyramidal neurons (PyNs). In areas such as the prelimbic cortex (PrL) of the medial prefrontal cortex (mPFC), layer V PyNs may receive significant input from CA1 and CA3 neurons in the hippocampus, with hyperexcitability. Additionally, these PyNs may display impaired counterbalance of inhibitory neurons, disrupting the E/I balance, and potentially resulting in AIS elongation and symptom manifestation. In the motor (MC) or sensory cortex (SC), relatively minor effect of hippocampal excitability combined with the counterbalance of inhibitory neurons via homeostatic mechanisms that may help to maintain normal AIS length and the excitatory/inhibitory (E/I) balance.

ASD, anxiety, epilepsy, sleep disorders, and motor disturbances [45–47]. Disturbances in the PrL are likely related to cognitive impairment, ASD, and anxiety.

In conclusion, this study showed that the AIS lengths of the layer V PyNs in the PrL of mKO and fKO mice were specifically altered through cell- and non-cell-autonomous mechanisms. A more detailed examination is necessary to reveal the mechanisms underlying neurocircuit abnormalities and the molecular mechanisms in *Ube3a*-deficient mice.

CRediT authorship contribution statement

Xinlang Liu: Writing – original draft, Methodology, Formal analysis, Data curation. **Zhuqian Jiang:** Writing – original draft, Methodology, Data curation. **Yoshinori Otani:** Writing – review & editing, Methodology, Funding acquisition. **Xiaowei Zhu:** Writing – review & editing, Methodology, Data curation. **Yanyan Yu:** Writing – review & editing, Methodology, Data curation. **Abu Md Mamun Tarif:** Writing – review & editing, Methodology. **Raihana Nasrin Ferdousy:** Writing – review & editing, Methodology. **Tatsuya Kishino:** Writing – review & editing, Methodology. **Masashi Fujitani:** Writing – review & editing, Writing – original draft, Funding acquisition, Conceptualization.

Funding sources

This work was supported by a Grant-in-Aid for Scientific Research (C) from the Japan Society for the Promotion of Science (23K07290) to M.F., a Grant-in-Aid for Scientific Research (C) from the Japan Society for the Promotion of Science (22K07868) to Y.O., and the SU Capacity Building Project Towards a Sustainable Society (S-SPRING, JPMJSP2155) to X.L.

Declaration of competing interest

The authors declare that they have no known competing financial

interests or personal relationships that could have appeared to influence the work reported in this paper.

Acknowledgments

We acknowledge the technical expertise of the Interdisciplinary Center for Science Research, Head Office for Research, and Academic Information of Shimane University, Japan. We gratefully acknowledge the work of the members of our laboratory, Dr. Shigefumi Yokota and Dr. Kenichiro Kuwako.

Appendix B. Supplementary data

Supplementary data to this article can be found online at <https://doi.org/10.1016/j.bbrc.2025.151429>.

References

- [1] L.M. Palmer, G.J. Stuart, Site of action potential initiation in layer 5 pyramidal neurons, *J. Neurosci.* 26 (2006) 1854–1863, <https://doi.org/10.1523/JNEUROSCI.4812-05.2006>.
- [2] M.H. Kole, S.U. Ilshner, B.M. Kampa, S.R. Williams, P.C. Ruben, G.J. Stuart, Action potential generation requires a high sodium channel density in the axon initial segment, *Nat. Neurosci.* 11 (2008) 178–186, <https://doi.org/10.1038/nn2040>.
- [3] M.H. Kole, J.J. Letzkus, G.J. Stuart, Axon initial segment Kv1 channels control axonal action potential waveform and synaptic efficacy, *Neuron* 55 (2007) 633–647, <https://doi.org/10.1016/j.neuron.2007.07.031>.
- [4] A. Lorincz, Z. Nusser, Cell-type-dependent molecular composition of the axon initial segment, *J. Neurosci.* 28 (2008) 14329–14340, <https://doi.org/10.1523/JNEUROSCI.4833-08.2008>.
- [5] H. Kuba, T.M. Ishii, H. Ohmori, Axonal site of spike initiation enhances auditory coincidence detection, *Nature* 444 (2006) 1069–1072, <https://doi.org/10.1038/nature05347>.
- [6] H. Kuba, Y. Oichi, H. Ohmori, Presynaptic activity regulates Na⁽⁺⁾ channel distribution at the axon initial segment, *Nature* 465 (2010) 1075–1078, <https://doi.org/10.1038/nature09087>.

- [7] M.S. Grubb, Y. Shu, H. Kuba, M.N. Rasband, V.C. Wimmer, K.J. Bender, Short- and long-term plasticity at the axon initial segment, *J. Neurosci.* 31 (2011) 16049–16055, <https://doi.org/10.1523/JNEUROSCI.4064-11.2011>.
- [8] N. Jamann, M. Jordan, M. Engelhardt, Activity-dependent axonal plasticity in sensory systems, *Neuroscience* 368 (2018) 268–282, <https://doi.org/10.1016/j.neuroscience.2017.07.035>.
- [9] N. Jamann, D. Dannehl, N. Lehmann, R. Wagener, C. Thielemann, C. Schultz, J. Staiger, M.H.P. Kole, M. Engelhardt, Sensory input drives rapid homeostatic scaling of the axon initial segment in mouse barrel cortex, *Nat. Commun.* 12 (2021) 23, <https://doi.org/10.1038/s41467-020-20232-x>.
- [10] N.M. George, A. Gentile Polese, L. Merle, W.B. Macklin, D. Restrepo, Excitable axonal domains adapt to sensory deprivation in the olfactory system, *J. Neurosci.* (2022), <https://doi.org/10.1523/JNEUROSCI.0305-21.2021>.
- [11] A. Gutzmann, N. Ergul, R. Grossmann, C. Schultz, P. Wahle, M. Engelhardt, A period of structural plasticity at the axon initial segment in developing visual cortex, *Front. Neuroanat.* 8 (2014) 11, <https://doi.org/10.3389/fnana.2014.00011>.
- [12] H.S. Jorgensen, D.B. Jensen, K.P. Dimintyanova, V.S. Bonnevie, A. Hedegaard, J. Lehnhoff, M. Moldovan, L. Grondahl, C.F. Meehan, Increased axon initial segment length results in increased Na⁺ currents in spinal motoneurons at symptom onset in the G127X SOD1 mouse model of amyotrophic lateral sclerosis, *Neuroscience* 468 (2021) 247–264, <https://doi.org/10.1016/j.neuroscience.2020.11.016>.
- [13] A. Anton-Fernandez, G. Leon-Espinosa, J. DeFelipe, A. Munoz, Pyramidal cell axon initial segment in Alzheimer's disease, *Sci. Rep.* 12 (2022) 8722, <https://doi.org/10.1038/s41598-022-12700-9>.
- [14] Y. Otani, K. Koga, R. Kawabata, X. Liu, H. Miyajima, T. Takumi, M. Fujitani, Aberrant axon initial segment is an indicator for task-independent neural activity in autism model mice, *bioRxiv* (2024), <https://doi.org/10.1101/2024.02.15.580571>.
- [15] N. Usui, X. Tian, W. Harigai, S. Togawa, R. Utsunomiya, T. Doi, K. Miyoshi, K. Shinoda, J. Tanaka, S. Shimada, T. Katayama, T. Yoshimura, Length impairments of the axon initial segment in rodent models of attention-deficit hyperactivity disorder and autism spectrum disorder, *Neurochem. Int.* 153 (2022) 105273, <https://doi.org/10.1016/j.neuint.2021.105273>.
- [16] S.A. Booker, L. Simoes de Oliveira, N.J. Anstey, Z. Kozic, O.R. Dando, A.D. Jackson, P.S. Baxter, L.L. Isom, D.L. Sherman, G.E. Hardingham, P.J. Brophy, D.J.A. Wyllie, P.C. Kind, Input-output relationship of CA1 pyramidal neurons reveals intact homeostatic mechanisms in a mouse model of fragile X syndrome, *Cell Rep.* 32 (2020) 107988, <https://doi.org/10.1016/j.celrep.2020.107988>.
- [17] H. Kaphzan, S.A. Buffington, J.I. Jung, M.N. Rasband, E. Klann, Alterations in intrinsic membrane properties and the axon initial segment in a mouse model of Angelman syndrome, *J. Neurosci.* 31 (2011) 17637–17648, <https://doi.org/10.1523/JNEUROSCI.4162-11.2011>.
- [18] N. Vatsa, N.R. Jana, UBE3A and its link with autism, *Front. Mol. Neurosci.* 11 (2018) 448, <https://doi.org/10.3389/fnmol.2018.00448>.
- [19] J.C. Krzeski, M.C. Judson, B.D. Philpot, Neuronal UBE3A substrates hold therapeutic potential for Angelman syndrome, *Curr. Opin. Neurobiol.* 88 (2024) 102899, <https://doi.org/10.1016/j.conb.2024.102899>.
- [20] M.C. Judson, J.O. Sosa-Pagan, W.A. Del Cid, J.E. Han, B.D. Philpot, Allelic specificity of Ube3a expression in the mouse brain during postnatal development, *J. Comp. Neurol.* 522 (2014) 1874–1896, <https://doi.org/10.1002/cne.23507>.
- [21] C.A. Williams, D.J. Driscoll, A.I. Dagli, Clinical and genetic aspects of Angelman syndrome, *Genet. Med.* 12 (2010) 385–395, <https://doi.org/10.1097/GIM.0b013e318181def138>.
- [22] S.S. Margolis, G.L. Sell, M.A. Zbinden, L.M. Bird, Angelman syndrome, *Neurotherapeutics* 12 (2015) 641–650, <https://doi.org/10.1007/s13311-015-0361-y>.
- [23] P.R. Rayi, A.Y. Bagrov, H. Kaphzan, Chronic alpha 1-Na/K-ATPase inhibition reverses the elongation of the axon initial segment of the hippocampal CA1 pyramidal neurons in Angelman syndrome model mice, *Neuropsychopharmacology* 46 (2021) 654–664, <https://doi.org/10.1038/s41386-020-00907-1>.
- [24] K. Miura, T. Kishino, E. Li, H. Webber, P. Dikkes, G.L. Holmes, J. Wagstaff, Neurobehavioral and electroencephalographic abnormalities in Ube3a maternal-deficient mice, *Neurobiol. Dis.* 9 (2002) 149–159, <https://doi.org/10.1006/nbdi.2001.0463>.
- [25] M.H. Longair, D.A. Baker, J.D. Armstrong, Simple Neurite Tracer: open source software for reconstruction, visualization and analysis of neuronal processes, *Bioinformatics* 27 (2011) 2453–2454, <https://doi.org/10.1093/bioinformatics/btr390>.
- [26] G. Zhong, J. He, R. Zhou, D. Lorenzo, H.P. Babcock, V. Bennett, X. Zhuang, Developmental mechanism of the periodic membrane skeleton in axons, *Elife* 3 (2014), <https://doi.org/10.7554/eLife.04581>.
- [27] M.R. Galiano, S. Jha, T.S. Ho, C. Zhang, Y. Ogawa, K.J. Chang, M.C. Stankewich, P. J. Mohler, M.N. Rasband, A distal axonal cytoskeleton forms an intra-axonal boundary that controls axon initial segment assembly, *Cell* 149 (2012) 1125–1139, <https://doi.org/10.1016/j.cell.2012.03.039>.
- [28] P.M. Jenkins, N. Kim, S.L. Jones, W.C. Tseng, T.M. Svitkina, H.H. Yin, V. Bennett, Giant ankyrin-G: a critical innovation in vertebrate evolution of fast and integrated neuronal signaling, *Proc. Natl. Acad. Sci. U.S.A.* 112 (2015) 957–964, <https://doi.org/10.1073/pnas.1416544112>.
- [29] A. Freal, C. Fassier, B. Le Bras, E. Bullier, S. De Gois, J. Hazan, C.C. Hoogenraad, F. Couraud, Cooperative interactions between 480 kDa ankyrin-G and EB proteins assemble the axon initial segment, *J. Neurosci.* 36 (2016) 4421–4433, <https://doi.org/10.1523/JNEUROSCI.3219-15.2016>.
- [30] H. Kaphzan, S.A. Buffington, A.B. Ramaraj, J.B. Lingrel, M.N. Rasband, E. Santini, E. Klann, Genetic reduction of the alpha 1 subunit of Na/K-ATPase corrects multiple hippocampal phenotypes in Angelman syndrome, *Cell Rep.* 4 (2013) 405–412, <https://doi.org/10.1016/j.celrep.2013.07.005>.
- [31] W. Zhang, Y. Fu, L. Peng, Y. Ogawa, X. Ding, A. Rasband, X. Zhou, M. Shelly, M. N. Rasband, P. Zou, Immunoprecipitation biotinylation reveals the axon initial segment proteome, *Nat. Commun.* 14 (2023) 8201, <https://doi.org/10.1038/s41467-023-44015-2>.
- [32] Y. Wang, X. Liu, L. Zhou, D. Duong, K. Bhuripanyo, B. Zhao, H. Zhou, R. Liu, Y. Bi, H. Kiyokawa, J. Yin, Identifying the ubiquitination targets of E6AP by orthogonal ubiquitin transfer, *Nat. Commun.* 8 (2017) 2232, <https://doi.org/10.1038/s41467-017-01974-7>.
- [33] S.Y. Lee, J. Ramirez, M. Franco, B. Lectez, M. Gonzalez, R. Barrio, U. Mayor, Ube3a, the E3 ubiquitin ligase causing Angelman syndrome and linked to autism, regulates protein homeostasis through the proteasomal shuttle Rpn10, *Cell. Mol. Life Sci.* 71 (2014) 2747–2758, <https://doi.org/10.1007/s00018-013-1526-7>.
- [34] A.X. Sun, Q. Yuan, M. Fukuda, W. Yu, H. Yan, G.G.Y. Lim, M.H. Nai, G. A. D'Agostino, H.D. Tran, Y. Itahana, D. Wang, H. Lokman, K. Itahana, S.W.L. Lim, J. Tang, Y.Y. Chang, M. Zhang, S.A. Cook, O.J.L. Rackham, C.T. Lim, E.K. Tan, H. H. Ng, K.L. Lim, Y.H. Jiang, H.S. Je, Potassium channel dysfunction in human neuronal models of Angelman syndrome, *Science* 366 (2019) 1486–1492, <https://doi.org/10.1126/science.aav5386>.
- [35] L. Filipis, L.A. Blomer, J. Montnach, G. Loussouarn, M. De Waard, M. Canepari, Nav 1.2 and BK channel interaction shapes the action potential in the axon initial segment, *J. Physiol.* 601 (2023) 1957–1979, <https://doi.org/10.1113/JP283801>.
- [36] D.C. Rotaru, G.M. van Woerden, I. Wallaard, Y. Elgersma, Adult Ube3a gene reinstatement restores the electrophysiological deficits of prefrontal cortex layer 5 neurons in a mouse model of Angelman syndrome, *J. Neurosci.* 38 (2018) 8011–8030, <https://doi.org/10.1523/JNEUROSCI.0083-18.2018>.
- [37] Michael L. Wallace, Alain C. Burette, Richard J. Weinberg, Benjamin D. Philpot, Maternal loss of Ube3a produces an excitatory/inhibitory imbalance through neuron type-specific synaptic defects, *Neuron* 74 (2012) 793–800, <https://doi.org/10.1016/j.neuron.2012.03.036>.
- [38] M. Inan, S.A. Anderson, The chandelier cell, form and function, *Curr. Opin. Neurobiol.* 26 (2014) 142–148, <https://doi.org/10.1016/j.conb.2014.01.009>.
- [39] W. Wefelmeyer, C.J. Puhl, J. Burrone, Homeostatic plasticity of subcellular neuronal structures: from inputs to outputs, *Trends Neurosci.* 39 (2016) 656–667, <https://doi.org/10.1016/j.tins.2016.08.004>.
- [40] K. Jung, Y. Choi, H.B. Kwon, Cortical control of chandelier cells in neural codes, *Front. Cell. Neurosci.* 16 (2022) 992409, <https://doi.org/10.3389/fncel.2022.992409>.
- [41] Y. Kawaguchi, T. Otsuka, M. Morishima, M. Ushimaru, Y. Kubota, Control of excitatory hierarchical circuits by parvalbumin-FS basket cells in layer 5 of the frontal cortex: insights for cortical oscillations, *J. Neurophysiol.* 121 (2019) 2222–2236, <https://doi.org/10.1152/jn.00778.2018>.
- [42] A. Tudi, M. Yao, F. Tang, J. Zhou, A. Li, H. Gong, T. Jiang, X. Li, Subregion preference in the long-range connectome of pyramidal neurons in the medial prefrontal cortex, *BMC Biol.* 22 (2024) 95, <https://doi.org/10.1186/s12915-024-01880-7>.
- [43] P.G. Anastasiades, A.G. Carter, Circuit organization of the rodent medial prefrontal cortex, *Trends Neurosci.* 44 (2021) 550–563, <https://doi.org/10.1016/j.tins.2021.03.006>.
- [44] P. Le Merre, S. Ahrlund-Richter, M. Carlen, The mouse prefrontal cortex: unity in diversity, *Neuron* 109 (2021) 1925–1944, <https://doi.org/10.1016/j.neuron.2021.03.035>.
- [45] D.C. Rotaru, E.J. Mientjes, Y. Elgersma, Angelman syndrome: from mouse models to therapy, *Neuroscience* 445 (2020) 172–189, <https://doi.org/10.1016/j.neuroscience.2020.02.017>.
- [46] E.L. Berg, S.A. Jami, S.P. Petkova, A. Berz, T.A. Fenton, J.P. Lerch, D.J. Segal, J. A. Gray, J. Ellegood, M. Wahr, J.L. Silverman, Excessive laughter-like vocalizations, microcephaly, and translational outcomes in the Ube3a deletion rat model of Angelman syndrome, *J. Neurosci.* 41 (2021) 8801–8814, <https://doi.org/10.1523/JNEUROSCI.0925-21.2021>.
- [47] M. Sonzogni, I. Wallaard, S.S. Santos, J. Kingma, D. du Mee, G.M. van Woerden, Y. Elgersma, A behavioral test battery for mouse models of Angelman syndrome: a powerful tool for testing drugs and novel Ube3a mutants, *Mol. Autism* 9 (2018) 47, <https://doi.org/10.1186/s13229-018-0231-7>.